Elasto-viscoplastic analysis for negative through-the-thickness Poisson's ratio of woven laminate composites based on homogenization theory

Keita Goto[a,*], Masahiro Arai[a], Tetsuya Matsuda[b], Gai Kubo[b]

[a] *Department of Aerospace Engineering, Nagoya University, Furo-cho, Chikusa-ku, Nagoya, 464–8603, Japan*
[b] *Department of Engineering Mechanics and Energy, University of Tsukuba, 1-1-1, Tennodai, Tsukuba, 305–8573, Japan*

Abstract

In this study, the negative through-the-thickness Poisson's ratios of $[\pm\theta]$ woven laminates were analyzed based on the homogenization theory for elasto-viscoplastic materials. A $[\pm\theta]$ woven laminate model with the fiber bundle cross angle $\pm\theta$ was considered and its diamond-shaped domain of analysis was defined. The elasto-viscoplastic homogenization analysis was performed to investigate the negativity of the through-the-thickness Poisson's ratios for the $[\pm\theta]$ carbon fiber/epoxy and glass fiber/epoxy woven laminates. The through-the-thickness Poisson's ratio of the $[\pm30^\circ]$ carbon fiber/epoxy woven laminate was negative in both the elastic and viscoplastic regions. However, that of the $[\pm30^\circ]$ glass fiber/epoxy woven laminate was positive in the elastic region but became negative in the viscoplastic region. The negative through-the-thickness Poisson's ratios of the $[\pm30^\circ]$ woven laminates were caused by the compressive stress with respect to the in-plane direction and

*goto@nuae.nagoya-u.ac.jp

the viscoplastic deformation of the matrix.

Keywords: Fiber-reinforced composite, Woven laminate, Multiscale analysis, Viscoplasticity, Negative Poisson's ratio

1. Introduction

During the last few decades, fiber-reinforced plastics (FRPs), which consist of reinforcing fibers and a matrix resin, have become indispensable materials, widely used in several industrial fields owing to their features, such as high specific strength and stiffness, to reduce the weight of structures. FRPs can be classified by the types of the reinforcing fibers and the matrix resins, the configurations of the reinforcing fibers, and so on. Among them, carbon fiber-reinforced plastic (CFRP) laminates made of unidirectionally reinforced prepregs have been used generally for the structural components of various industrial products. However, textile composites reinforced by three-dimensional woven fabrics, such as plain-woven laminates, are also important because of their high impact resistance and good formability.

From the viewpoint of the increasing demand for FRPs in the industrial fields, it is indispensable to understand their mechanical behavior in detail. It is generally known the FRPs show complex mechanical behavior because they are made of reinforcing fibers and a matrix resin, which show extremely different material properties. Moreover, the mechanical behavior of the FRPs is affected by their microscopic internal structures. Such inhomogeneity of the FRPs can cause strong anisotropy of the mechanical properties. In particular, it has been reported the Poisson's ratios of FRPs can show not only anisotropy but also negativity. The negative Poisson's ratios of CFRP lami-

nates were originally investigated by Herakovich [1]. In that study, the Poisson's ratios of T300/5208 angle-ply CFRP laminates were analyzed using a two-dimensional lamination theory. The through-the-thickness Poisson's ratios of the laminates were between approximately 0.5 and -0.2, depending on the stacking sequences. Clarke et al. [2] investigated the negative Poisson's ratios of CFRP laminates, not only analytically but also experimentally, with an ultrasonic velocity measurement technique. Moreover, Harkati et al. [3] researched the effect of the types of reinforcing fibers on the Poisson's ratios of laminates. They revealed that the through-the-thickness Poisson's ratios of carbon fiber/epoxy and Kevlar/epoxy angle-ply laminates become negative, but that of the glass fiber/epoxy one does not show the negative through-the-thickness Poisson's ratio.

Because the above-mentioned studies were limited to the elastic analyses, the effect of the matrix nonlinearity on the negative Poisson's ratios has not been clarified. Moreover, they were based on the classical lamination theory. The theory assumes each prepreg as a homogeneous material, and thus the microscopic mechanism of the negative Poisson's ratios has not been discussed in detail. To solve these problems, the authors have investigated the negative Poisson's ratios of angle-ply CFRP laminates in the elastic and viscoplastic regions using the homogenization theory for elasto-viscoplastic materials [4]. It was revealed that the negativity of the through-the-thickness Poisson's ratios for the angle-ply laminates becomes greater with increasing viscoplastic deformation of the matrix, and such a negative Poisson's ratio is caused by the induced compressive microscopic stress in the transverse fiber directions in each prepreg. In addition, the authors have analyzed the

effect of the fiber arrangement on the elasto-viscoplastic negative Poisson's ratios of the angle-ply CFRP laminates [5]. As mentioned here, the negative Poisson's ratios of FRP laminates consisting of unidirectionally-reinforced prepregs have been investigated by some researchers. Similarly, the woven composites of which fiber bundles are crossed nonorthogonally, for example the structures made by the filament winding technique or slanting-weft loom machines [6, 7], would also show negative through-the-thickness Poisson's ratios.

A homogenization theory based on a unit cell analysis [8, 9, 10] is one of the most useful theories to analyze the mechanical properties of heterogeneous materials, such as semicrystalline polymers [11, 12, 13], plate- or tube-fin structures [14, 15, 16], and composites [17, 18, 19]. The theory can analyze the macroscopic mechanical properties of heterogeneous materials from the microscopic structures and the constitutive equations of their constituent materials. Moreover, the inelastic behavior of heterogeneous materials can also be considered by introducing nonlinear constitutive equations [20, 21]. The homogenization theory with nonlinear constitutive equations have been applied to inelastic analyses of composite materials, elasto-viscoplastic [22, 23], thermo-viscoplastic [24] and creep analyses [25] of CFRP laminates made of unidirectionally-reinforced prepregs and glass fiber-reinforced plain-woven laminates [26, 27]. The negative Poisson's ratio of the woven laminates, thus, could be investigated using a numerical method based on the homogenization theory proposed in the previous study [26, 27].

In this study, the negative through-the-thickness Poisson's ratios of $[\pm\theta]$ woven laminates are analyzed based on the homogenization theory for elasto-

viscoplastic materials. The $[\pm\theta]$ woven laminate model consisting of fiber bundles with arbitrary cross angles $\pm\theta$ and a matrix is considered, and its diamond-shaped domain of analysis is defined. Then, a nonlinear numerical method based on the homogenization theory with point-symmetric internal structures [26, 28] is applied to the laminates to demonstrate their elasto-viscoplastic behavior, including negative Poisson's ratios. Two types of the woven laminates, carbon fiber/epoxy and glass fiber/epoxy woven laminates, are considered to investigate the effects of the mechanical properties of the woven laminates on the through-the-thickness Poisson's ratios. Finally, the microscopic mechanism for the negative Poisson's ratios of the $[\pm\theta]$ woven laminates is discussed based on the microscopic stress distribution.

2. Numerical method

2.1. Modeling of $[\pm\theta]$ *woven laminate*

Let us consider a $[\pm\theta]$ woven laminate consisting of fiber bundles and a matrix, as shown in Fig. 1, and the Cartesian coordinates y_i $(i = 1, 2, 3)$ are defined. The fiber bundles of the laminate are woven together with a cross angle $\pm\theta$ from the y_1-direction. For the laminate, a diamond-shaped unit cell Y can be defined as shown in Fig. 1. In the present formulation, the quarter part of the unit cell can also be defined as a domain of analysis by considering the point-symmetry of the internal structure [26, 28]. Thus, the quarter part of the unit cell is employed in this study. Hereafter, this quarter part of the unit cell is called basic cell A.

2.2. Homogenization theory for elasto-viscoplastic materials with point-symmetry

Basic cell A are assumed to exhibit linear elasticity and nonlinear viscoplasticity as characterized by

$$\dot{\sigma}_{ij} = c_{ijkl}(\dot{\varepsilon}_{kl} - \beta_{kl}), \tag{1}$$

where σ_{ij} and ε_{ij} denote the microscopic stress and strain defined in basic cell A, respectively. Here, $(\dot{})$ stands for the differentiation with respect to time t. Moreover, c_{ijkl} and β_{ij} indicate the elastic stiffness and the viscoplastic strain rate satisfying $c_{ijkl} = c_{jikl} = c_{ijlk} = c_{klij}$ and $\beta_{ij} = \beta_{ji}$, respectively. Then, the homogenization theory for elasto-viscoplastic materials with point-symmetric microscopic internal structures [28, 26] gives the evolution equation of σ_{ij} and the relation between the macroscopic stress and strain rates, $\dot{\Sigma}_{ij}$ and $\dot{E}_{ij}$, as follows:

$$\dot{\sigma}_{ij} = c_{ijpq}(\delta_{pk}\delta_{ql} + \chi^{kl}_{p,q})\dot{E}_{kl} - c_{ijkl}(\beta_{kl} - \varphi_{k,l}), \tag{2}$$

$$\dot{\Sigma}_{ij} = \left\langle c_{ijpq}(\delta_{pk}\delta_{ql} + \chi^{kl}_{p,q})\right\rangle \dot{E}_{kl} - \left\langle c_{ijkl}(\beta_{kl} - \varphi_{k,l})\right\rangle, \tag{3}$$

where δ_{ij} indicates Kronecker's delta, $(\ )_{,i}$ denotes the differentiation with respect to y_i, and $\langle\ \rangle$ designates the volume average in A defined as $\langle \sharp \rangle = |A|^{-1}\int_A \sharp dA$, in which $|A|$ signifies the volume of A. Moreover, χ^{kl}_i and φ_i are the characteristic functions determined by solving the following boundary value problems [26];

$$\int_A c_{ijpq}\chi^{kl}_{p,q}v_{i,j}dA = -\int_A c_{ijkl}v_{i,j}dA, \tag{4}$$

$$\int_A c_{ijpq}\varphi_{p,q}v_{i,j}dA = \int_A c_{ijkl}\beta_{kl}v_{i,j}dA, \tag{5}$$

where v_i indicates an arbitrary variation of a perturbed velocity field satisfying the point-symmetry with respect to the centers of the lateral facets of A. The boundary value problems (4) and (5) can usually be solved by the finite element method with suitable boundary conditions with respect to A. After the calculation of χ_i^{kl} and φ_i, the microscopic stress distribution in A and the macroscopic elasto-viscoplastic behavior of the laminate can be analyzed by the time-integral calculation, based on Eqs. (2) and (3) from the time-history of $\dot{\Sigma}_{ij}$ or $\dot{E}_{ij}$, or a combination of them.

3. Numerical models and parameters

3.1. Finite element models

The numerical models of the $[\pm\theta]$ woven laminates were made based on the basic cells A for the typical $[0°/90°]$ plain-woven laminates. In this study, two types of the woven laminates, carbon fiber/epoxy and glass fiber/epoxy woven laminates, were considered to investigate the effect of the mechanical properties on the Poisson's ratios. The carbon fiber/epoxy and glass fiber/epoxy woven laminates are hereafter called the CF and GF woven laminates, respectively. The finite element model of the basic cell A of the $[0°/90°]$ CF plain-woven laminate is illustrated in Fig. 2(a). In addition, Fig. 2(b) shows the cross section at the center of A indicated by the solid and dashed lines in Fig. 2(a). The finite element model of the basic cell A of the $[0°/90°]$ GF plain-woven laminate and its cross section are also depicted in Figs 2(c) and (d), respectively. The dimensions of A for the CF plain-woven laminate were determined from microscopy of the laminates made of TR3110/381GMX prepregs (Mitsubishi Rayon Co., Ltd.). However, that

for the GF plain-woven laminate were defined based on the previous study by Matsuda et al. [26, 27]. These models were discretized into eight-node isoparametric elements. The numbers of nodes and elements were 4011/3360 for the CF woven laminate, and 2499/2048 for the GF woven laminate. The volume fractions of the fiber bundles were 61.7% and 50.8% for the CF and GF woven laminates, respectively. Each prepreg was assumed to be stacked with the phase shift by π, i.e., the out-of-phase lamination [26], to consider misalignments in the laminates. The point-symmetric boundary condition was applied for all boundary facets of the basic cell A. Three fiber bundle cross angles $\pm\theta$ for the $[\pm\theta]$ woven laminates, $\theta = 30°$, $45°$ and $60°$, were considered. The basic cells A of the $[\pm\theta]$ CF and GF woven laminates are shown in Figs. 3 and 4. It is noted that the basic cells A of the $[\pm 45°]$ woven laminates are omitted from these figures because they have the same shapes as the $[0°/90°]$ woven laminates rotated by $45°$ with respect to the y_3-direction.

3.2. Material parameters

The fiber bundles were composed of reinforcing fibers and an epoxy matrix and regarded as a transversely-isotropic elastic material. The volume fraction of the fibers in the fiber bundles was set to 75% for both the woven laminates. However, the epoxy matrix was assumed to be an isotropic elasto-viscoplastic material obeying the following elasto-viscoplastic constitutive equation:

$$\dot{\varepsilon}_{ij} = \frac{1+\nu}{E}\dot{\sigma}_{ij} - \frac{\nu}{E}\dot{\sigma}_{kk}\delta_{ij} + \frac{3}{2}\dot{\varepsilon}_0^p \left[\frac{\sigma_e}{g(\bar{\varepsilon}^p)}\right]^n \frac{s_{ij}}{\sigma_e}, \tag{6}$$

where $g(\bar{\varepsilon}^p)$ denotes a hardening function depending on the accumulated viscoplastic strain $\bar{\varepsilon}^p$, $\dot{\varepsilon}_0^p$ indicates a reference strain rate, s_{ij} stands for the

deviatoric part of σ_{ij}, and $\sigma_e = [(3/2)s_{ij}s_{ij}]^{1/2}$.

To identify the material parameters of the CF woven laminates, uniaxial tensile tests of the [0°/90°] carbon fiber/epoxy plain-woven laminates made of TR3110/381GMX prepregs (Mitsubishi Rayon Co., Ltd.) were performed under on- and off-axes loadings with several strain rates. The experimental results of the uniaxial tensile tests are shown in Figs. 5 and 6 by the filled and open circles. Fig. 5 shows the relation between the macroscopic stress Σ_ψ and strain E_ψ subjected to the on- and off-axes in-plane tensile loadings at the macroscopic tensile strain rate $\dot{E}_\psi = 10^{-5}$ s^{-1}. Here, ψ denotes the off-axis angle between the loading direction and the y_1-direction in the y_1-y_2 plane. In addition, Fig. 6 shows the relation between Σ_ψ and E_ψ subjected to the off-axis loading $\psi = 45°$ at $\dot{E}_\psi = 10^{-3}$ s^{-1} and 10^{-5} s^{-1}. Based on these experimental results, the material parameters of the CF woven laminates were identified by trial-and-error fittings. The identified material parameters of the CF woven laminates are listed in Table 1. The numerical results of the relation between Σ_ψ and E_ψ of the [0°/90°] CF woven laminates are shown in Figs. 5 and 6 by the solid and dashed lines. The material parameters of the GF woven laminates shown in Table 2 were used as identified by Matsuda et al. [26]. It is noted the subscripts L and T in the tables denote the longitudinal and transverse directions of the fiber bundles, respectively.

4. Results and discussion

4.1. Macroscopic and microscopic mechanical behavior of woven laminates

The relations between the macroscopic stress and strain of the CF and GF woven laminates for three fiber bundle cross angles, [±30°], [±45°], and

$[\pm 60^\circ]$, subjected to a uniaxial tensile strain rate $\dot{E}_{11} = 10^{-5}\ \mathrm{s}^{-1}$ are shown in Figs. 7 and 8. Here, the number of time steps in these numerical demonstrations was set as 15000 for the CF and GF woven laminates up to $E_{11} = 0.015$ for all strain rate conditions. All the laminates exhibit clear nonlinearity as the macroscopic strain E_{11} increases. Moreover, the stress levels drop remarkably as the fiber bundle cross angle increases from $[\pm 30^\circ]$ to $[\pm 45^\circ]$ for both the CF and GF woven laminates, owing to the anisotropy of the fiber bundles. The same tendency can also be observed for the initial elastic modulus of the basic cells A with respect to the y_1-direction, as shown in these figures.

However, the $[\pm 45^\circ]$ and $[\pm 60^\circ]$ GF woven laminates show an opposite behavior in the viscoplastic region. In the elastic and the initial viscoplastic regions, the stress level of the $[\pm 45^\circ]$ GF woven laminate is high compared with that of the $[\pm 60^\circ]$ GF woven laminate. The stress level of the $[\pm 60^\circ]$ GF woven laminate then increases gradually with further increase in the macroscopic strain E_{11}, although that of the $[\pm 45^\circ]$ GF woven laminate is almost saturated, and finally the stress level of the $[\pm 60^\circ]$ GF woven laminate becomes higher than that of the $[\pm 45^\circ]$ GF woven laminate at the macroscopic strain $E_{11} > 0.011$. This is because the viscoplastic deformation of the epoxy matrix occurs widely for the $[\pm 45^\circ]$ GF woven laminate, especially at the crossover section of the upper and lower fiber bundles, owing to the rotation of the fiber bundles.

Now, the microscopic stress distributions in the basic cells A are focused on to investigate the effects of the types of fiber bundles or the cross angles $\pm\theta$ on their mechanical properties. The distributions of the microscopic Mises

equivalent stress in A and the fiber bundles for the [±30°] and [±60°] CF woven laminates are shown in Fig. 9, and those for the [±30°] and [±60°] GF woven laminates are illustrated in Fig. 10 at the macroscopic strain $E_{11} = 0.015$. The distributions of the microscopic stress are very different depending on the fiber bundle cross angles $\pm\theta$, similar to the relation between the macroscopic stress and strain shown in Figs. 7 and 8. For the [±30°] CF and GF woven laminates, high stress distributes at the fiber bundles because the angle between the longitudinal direction of the fiber bundles and the macroscopic loading direction is small. Therefore, the relations between macroscopic stress and strain for the [±30°] woven laminates showed higher values compared with the [±45°] and [±60°] woven laminates. Moreover, local stress concentrations at the edges of the fiber bundles can be found for the [±30°] CF woven laminate, whereas the stress distribution for the [±30°] GF woven laminate is relatively smooth, depending on the shapes of the fiber bundles.

4.2. Elasto-viscoplastic Poisson's ratios

The elasto-viscoplastic through-the-thickness and in-plane Poisson's ratios ν_{13}^{evp} and ν_{12}^{evp}, which are the indices with respect to the ratios of the macroscopic strains in the y_3- and y_2-directions, E_{33} and E_{22}, to that in the y_1-direction E_{11}, were newly introduced and respectively defined as follows [4, 5]:

$$\nu_{13}^{evp} = -\frac{E_{33}}{E_{11}}, \tag{7}$$

$$\nu_{12}^{evp} = -\frac{E_{22}}{E_{11}}. \tag{8}$$

The relations between the macroscopic strain E_{11} and the elasto-viscoplastic Poisson's ratios ν_{13}^{evp} and ν_{12}^{evp} for the [±30°], [±45°], and [±60°] CF woven laminates are shown in Figs. 11 and 12. As shown in Fig. 11, the through-the-thickness Poisson's ratio ν_{13}^{evp} of the [±30°] CF woven laminate shows negativity in all regions of the macroscopic strain E_{11}. In addition, the negativity of ν_{13}^{evp} of the [±30°] CF woven laminate increases from approximately -0.1 to -0.5 with increasing macroscopic strain E_{11}. Corresponding to the negative through-the-thickness Poisson's ratio ν_{13}^{evp}, the in-plane Poisson's ratio ν_{12}^{evp} of the [±30°] CF woven laminate increases over 1.2, as shown in Fig. 12. In contrast, the Poisson's ratios ν_{13}^{evp} and ν_{12}^{evp} for the other two CF woven laminates are always positive and almost constant in both the elastic and viscoplastic regions.

However, Figs. 13 and 14 indicate the variation of the elasto-viscoplastic Poisson's ratios ν_{13}^{evp} and ν_{12}^{evp} for the [±30°], [±45°], and [±60°] GF woven laminates. From Fig. 13, it can be observed that the through-the-thickness Poisson's ratio ν_{13}^{evp} of the [±30°] GF woven laminate is positive, and almost equal to that of the [±45°] GF woven laminate, in the elastic region. However, the value of ν_{13}^{evp} for the [±30°] GF woven laminate decreases gradually and then becomes negative with increasing macroscopic strain E_{11}, although ν_{13}^{evp} for the [±45°] GF woven laminate remains positive. In addition, the opposite tendency, i.e., slightly increasing of ν_{13}^{evp} from approximately 0.3 to 0.4 for the [±60°] GF woven laminate can be found in the viscoplastic region. According to the decrease in the through-the-thickness Poisson's ratio ν_{13}^{evp}, the in-plane Poisson's ratios ν_{12}^{evp} for the [±30°] and [±45°] GF woven laminates increase in the viscoplastic region, whereas that of the [±60°] GF woven laminate

is almost constant. The increasing rate of ν_{12}^{evp} for the [±30°] GF woven laminate is larger than that of the [±45°] GF woven laminate, similar to the decreasing rate of ν_{13}^{evp}.

Harkati et al. reported that carbon fiber/epoxy and Kevlar/epoxy angle-ply laminates showed negative through-the-thickness Poisson's ratios in specific stacking sequences, but the Poisson's ratio of the glass fiber/epoxy laminate was always positive regardless of the stacking sequences [3]. However, the numerical results obtained in the present study suggest that the through-the-thickness Poisson's ratios of glass fiber/epoxy laminates can also become negative. Harkati et al. also mentioned that the negativity of the through-the-thickness Poisson's ratios strongly depended on the anisotropy of the composite materials [3]. The numerical results shown in Figs. 11 and 13 exhibit the same tendency, whereby the negativity of ν_{13}^{evp} for the [±30°] CF woven laminate, which shows the stronger anisotropy, is higher than that of the [±30°] GF woven laminate.

4.3. Microscopic mechanism of negative Poisson's ratio

The microscopic stress distribution is investigated to clarify the microscopic mechanism of the negative through-the-thickness Poisson's ratios of $[\pm\theta]$ woven laminates. Fig. 15 is the distribution of the microscopic stress σ_{22} for the [±30°] and [±60°] CF woven laminates at the macroscopic strain $E_{11} = 0.015$. The opposite stress distribution at the matrix around the basic cell A can be found. The compressive stress distributes for the [±30°] CF woven laminate, whereas the tensile stress distributes for the [±60°] CF woven laminate. Such compressive stress can induce the positive strain in the orthogonal directions owing to Poisson's effect. However, expansion in

the in-plane direction is inhibited by the fiber bundles. On account of these effects, the positive strain occurs remarkably in the through-the-thickness direction and such positive strain causes the negative through-the-thickness Poisson's ratio of the [±30°] CF woven laminates.

The distribution of the microscopic stress σ_{22} for the [±30°] and [±60°] GF woven laminates at the macroscopic strain $E_{11} = 0.015$ is also depicted in Fig. 16. Compared with the results of the $[\pm\theta]$ CF woven laminates, a similar distribution can be found for the $[\pm\theta]$ GF woven laminates. Nevertheless, the stress levels of σ_{22} are very different between the CF and GF woven laminates. The value of the compressive stress σ_{22} for the [±30°] CF laminate is approximately 80 MPa, which is approximately two times higher than that for the [±30°] GF woven laminate. Thus, it can be suggested that the negativity of the through-the-thickness Poisson's ratios is affected by the magnitude of the in-plane compressive stress owing to the anisotropy of the laminates. Moreover, the in-plane compressive stress induces further positive strain in the viscoplastic region with the progress of viscoplastic deformation of the matrix. This results in the increasing negativity or decreasing positivity of the through-the-thickness Poisson's ratios For the [±30°] CF or GF woven laminates, as reported by Matsuda et al. [4].

5. Conclusions

In this study, the negative through-the-thickness Poisson's ratios of the $[\pm\theta]$ woven laminates were analyzed based on the homogenization theory for elasto-viscoplastic materials with point-symmetric internal structures. The $[\pm\theta]$ woven laminate model consisting of fiber bundles and a matrix was

considered, and its diamond-shaped domain of analysis was defined. Two types of woven laminates, carbon fiber/epoxy and glass fiber/epoxy woven laminates, were considered to investigate the effect on the negative through-the-thickness Poisson's ratios of the $[\pm\theta]$ woven laminates.

From the numerical results, the through-the-thickness Poisson's ratio was negative in both the elastic and viscoplastic regions for the $[\pm 30^\circ]$ carbon fiber/epoxy woven laminate. In contrast, that of the $[\pm 30^\circ]$ glass fiber/epoxy woven laminate was positive in the elastic region, but it decreased and then became negative as the macroscopic strain increased. The negativity of the Poisson's ratios was strongly affected by the anisotropy of the laminates. From the results of the microscopic investigations, it was revealed the negative through-the-thickness Poisson's ratios were caused by the compressive stress with respect to the in-plane direction perpendicular to the loading direction. Moreover, the increasing negativity or decreasing positivity of the through-the-thickness Poisson's ratios was induced by the viscoplastic deformation of the matrix.

References

[1] Herakovich CT. Composite laminates with negative through-the-thickness Poisson's ratios. J Compos Mater 1984;18:447-55.

[2] Clarke JF, Duckett RA, Hine PJ, Hutchinson IJ, Ward IM. Negative Poisson's ratios in angle-ply laminates: theory and experiment. Composites 1994;25:863-8.

[3] Harkati EH, Bezazi A, Scarpa F, Alderson K, Alderson A. Modelling

the influence of the orientation and fibre reinforcement on the negative Poisson's ratio in composite laminates. Phys Status Sollidi B-Basic Solid State Phys 2007;244:883-92.

[4] Matsuda T, Goto K, Kubota N, Ohno N. Negative through-the-thickness Poisson's ratio of elastic-viscoplastic angle-ply carbon fiber-reinforced plastic laminates: Homogenization analysis. Int J Plast 2014;63:152-69.

[5] Matsuda T, Goto K, Ohno N. Effects of fiber arrangement on negative Poisson's ratio of angle-ply CFRP laminates: Analysis based on a homogenization theory. Adv Struct Mater 2015;64:219-30.

[6] Mertiny P, Ellyin F, Hothan A. An experimental investigation on the effect of multi-angle filament winding on the strength of tubular composite structures. Compos Sci Technol 2004;64:1-9.

[7] Almeida Jr JHS, Ribeiro ML, Tita V, AmicoSC. Damage modeling for carbon fiber/epoxy filament wound composite tubes under radial compression. Compos Struct 2017;160:204-10.

[8] Bensoussan A, Lions JL, Papanicolau G. Asymptotic Analysis for Periodic Structures. Amsterdam: North Holland;1978.

[9] Sanchez-Palencia E. Non-homogeneous media and vibration theory. Lecture Notes in Physics, vol. 127. Berlin: Springer-Verlag; 1980.

[10] Suquet PM. Elements of homogenization for inelastic solid mechanics. In: Sanchez-Palencia E., Zaoui A. editors. Lecture Notes in Physics, vol. 272. Berlin: Springer-Verlag; 1987.

[11] Tomita Y, Uchida M. Computational characterization of micro- to mesoscopic deformation behavior of semicrystalline polymers. Int J Mech Sci 2005;47:687-700.

[12] Uchida M, Tada N. Micro-, meso- to macroscopic modeling of deformation behavior of semi-crystalline polymer. Int J Plast 2013;49:164-184.

[13] Hara H, Shizawa K. Homogenized molecular chain plasticity simulation for crystalline polymer using craze evolution model based on chemical kinetics. Int J Mech Sci 2015;101-2:180-95.

[14] Ohno N, Narita K, Okumura D. Homogenized elastic-viscoplastic behavior of plate-fin structures with two pore pressures Int J Mech Sci 2014;86:18-25.

[15] Matsuda T, Ito T, Akimoto S, Kobori H, Goto K, Takano N. Macro/micro simultaneous validation for multiscale analysis of semi-periodically perforated plate using full-field strain measurement. Int J Mech Sci 2016;110:34-40.

[16] Okumura D, Ohno N, Iwahori K, Kamakura K, Miyakawa S. Homogenization of fin layers in tube-fin structures subjected to compression and bending: Analyses and experiments. Int J Mech Sci 2016;115-6:348-59.

[17] Takano N, Uetsuji Y, Kashiwagi Y, Zako M. Hierarchical modelling of textile composite materials and structures by the homogenization method. Model Simul Mater Sci Eng 1999;7:207-31.

[18] Terada K, Kikuchi N. A class of general algorithms for multi-scale

analyses of heterogeneous media. Comput Meth Appl Mech Eng 2001;190:5427-64.

[19] Carvelli V, Poggi C. A homogenization procedure for the numerical analysis of woven fabric composites. Compos Pt A-Appl Sci Manuf 2001;32:1425-32.

[20] Wu X, Ohno N. A homogenization theory for time-dependent nonlinear composites with periodic internal structures. Int J Solids Struct 1999;36:4991-5012.

[21] Ohno N, Wu X, Matsuda T. Homogenized properties of elastic-viscoplastic composites with periodic internal structures. Int J Mech Sci 2000;42:1519-36.

[22] Matsuda T, Ohno N, Tanaka H, Shimizu T. Homogenized in-plane elastic-viscoplastic behavior of long fiber-reinforced laminates. JSME Int J Ser A 2002;45:538-44.

[23] Matsuda T, Ohno N, Tanaka H, Shimizu T. Effects of fiber distribution on elastic-viscoplastic behavior of long fiber-reinforced laminates. Int J Mech Sci 2003;45:1583-98.

[24] Kaku K, Arai M, Fukuoka T, Matsuda T. Evaluation of thermo-viscoplastic property of CFRP laminate based on a homogenization theory. Acta Mech 2010;214:111-21.

[25] Matsuda T, Fukuta Y. Multi-scale creep analysis of angle-ply CFRP laminates based on a homogenization theory. J Solid Mech Mater Eng 2010;4:1664-72.

[26] Matsuda T, Nimiya Y, Ohno N, Tokuda M. Elastic–viscoplastic behavior of plain-woven GFRP laminates: Homogenization using a reduced domain of analysis. Compos Struct 2007;79:493-500.

[27] Matsuda T, Kanamaru S, Yamamoto N, Fukuda Y. A homogenization theory for elastic-viscoplastic materials with misaligned internal structures. Int J Plast 2011;27:2056-67.

[28] Ohno N, Matuda T, Wu X. A homogenization theory for elastic-viscoplastic composites with point symmetry of internal distributions. Int J Solids Struct 2001;38:2867-78.

Table 1: Material parameters of carbon fiber-reinforced woven laminate.

Fiber bundle	E_{LL}	176.34 [GPa]
(Carbon fiber/Epoxy)	E_{TT}	15.738 [GPa]
	G_{LT}	6.235 [GPa]
	ν_{LT}	0.219
	ν_{TT}	0.372
Epoxy	E	4.0 [GPa]
	ν	0.300
	$\dot{\varepsilon}_0^p$	10^{-5} [s^{-1}]
	n	25.0
	$g(\bar{\varepsilon}^p)$	$17.0 - 16.0 \exp(-190.0\bar{\varepsilon}^p)$ [MPa]

Table 2: Material parameters of glass fiber-reinforced woven laminate [26].

Fiber bundle	E_{LL}	61.0 [GPa]
(Glass fiber/Epoxy)	E_{TT}	25.8 [GPa]
	G_{LT}	9.35 [GPa]
	ν_{LT}	0.310
	ν_{TT}	0.355
Epoxy	E	5.0 [GPa]
	ν	0.350
	$\dot{\varepsilon}_0^p$	10^{-5} [s^{-1}]
	n	20.0
	$g(\bar{\varepsilon}^p)$	$(\bar{\varepsilon}^p)^{0.50} + 24.5/2.5^{(\bar{\varepsilon}^p)}$ [MPa]

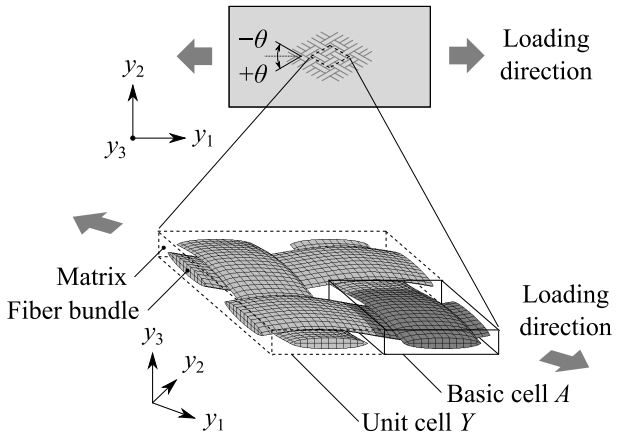

Figure 1: Unit cell and basic cell of $[\pm\theta]$ woven laminate.

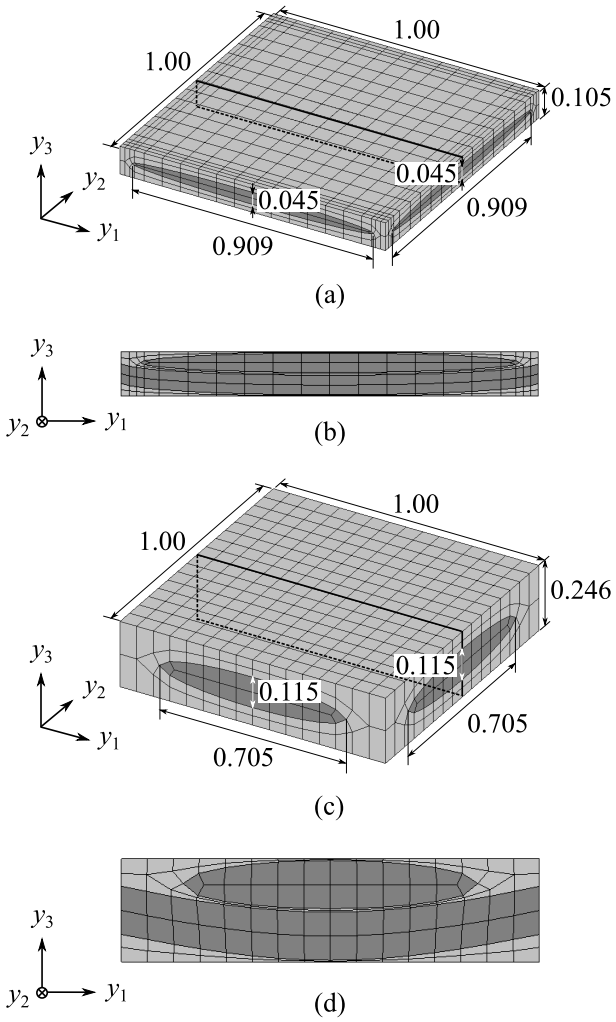

Figure 2: Finite element models of basic cells A; (a) [0°/90°] CF plain-woven laminate and (b) its cross section; (c) [0°/90°] GF plain-woven laminate and (d) its cross section.

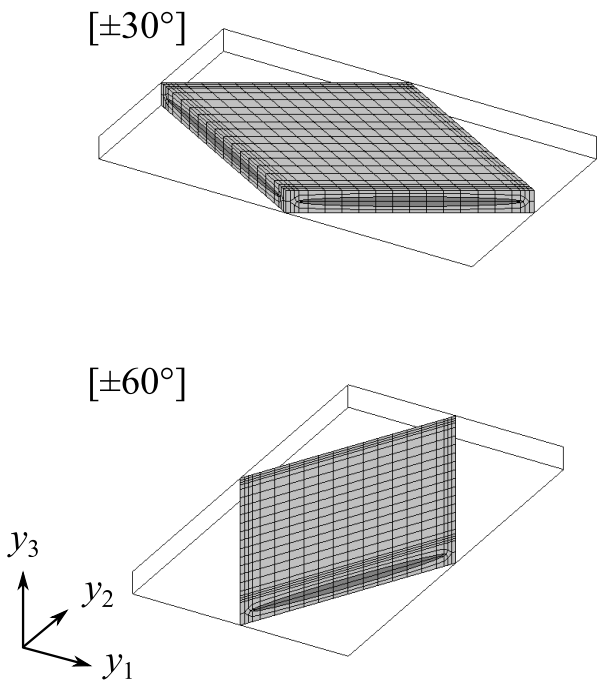

Figure 3: Basic cells A of [±30°] and [±60°] CF woven laminates.

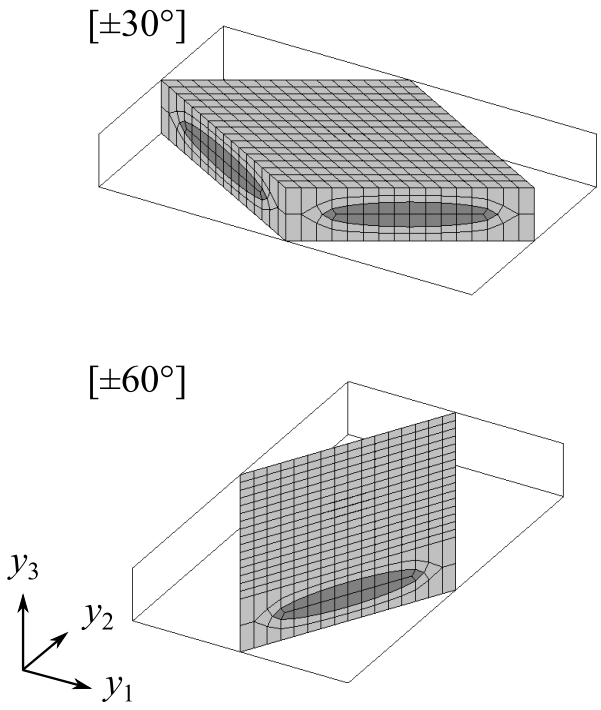

Figure 4: Basic cells A of [±30°] and [±60°] GF woven laminates.

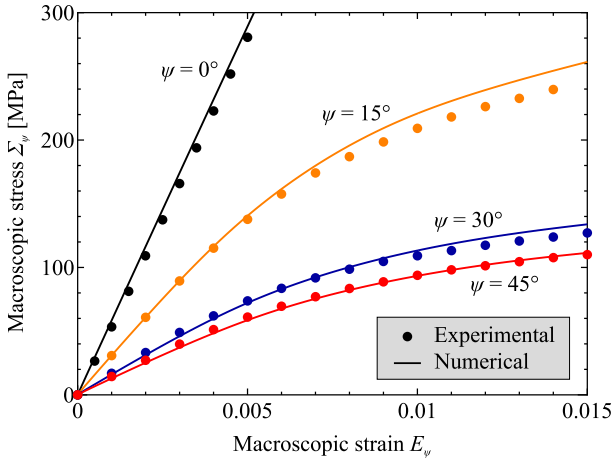

Figure 5: Relation between macroscopic stress and strain for [0°/90°] CF plain-woven laminate subjected to on- and off-axes loadings ($\dot{E}_\psi = 10^{-5}$ s^{-1}).

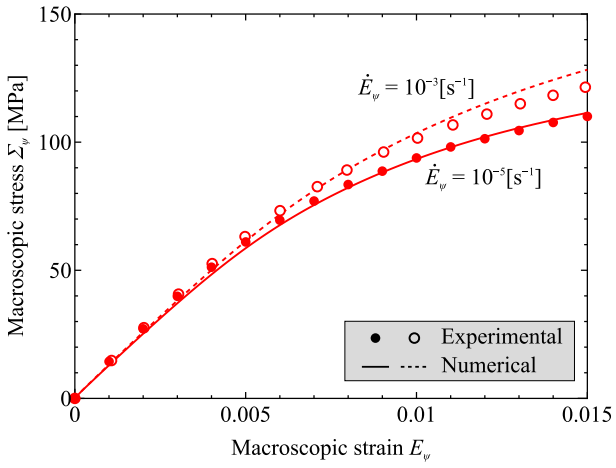

Figure 6: Relation between macroscopic stress and strain for [0°/90°] CF plain-woven laminate subjected to off-axis loading at $\dot{E}_\psi = 10^{-3}$ s^{-1} and 10^{-5}s^{-1} ($\psi = 45°$).

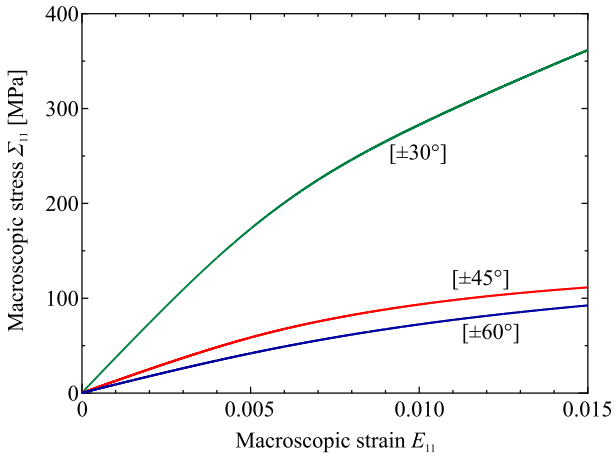

Figure 7: Relation between macroscopic stress and strain for [$\pm\theta$] CF woven laminates.

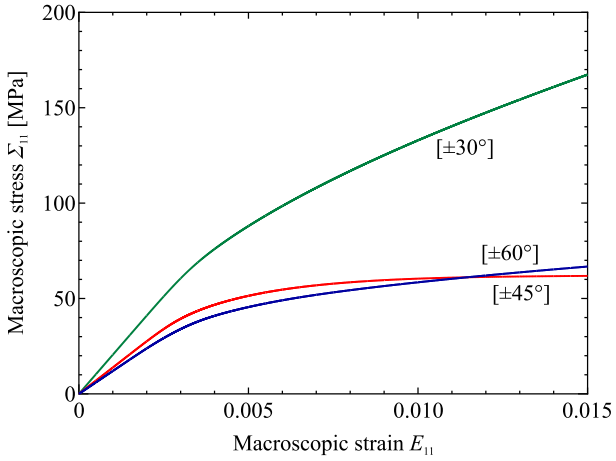

Figure 8: Relation between macroscopic stress and strain for $[\pm\theta]$ GF woven laminates.

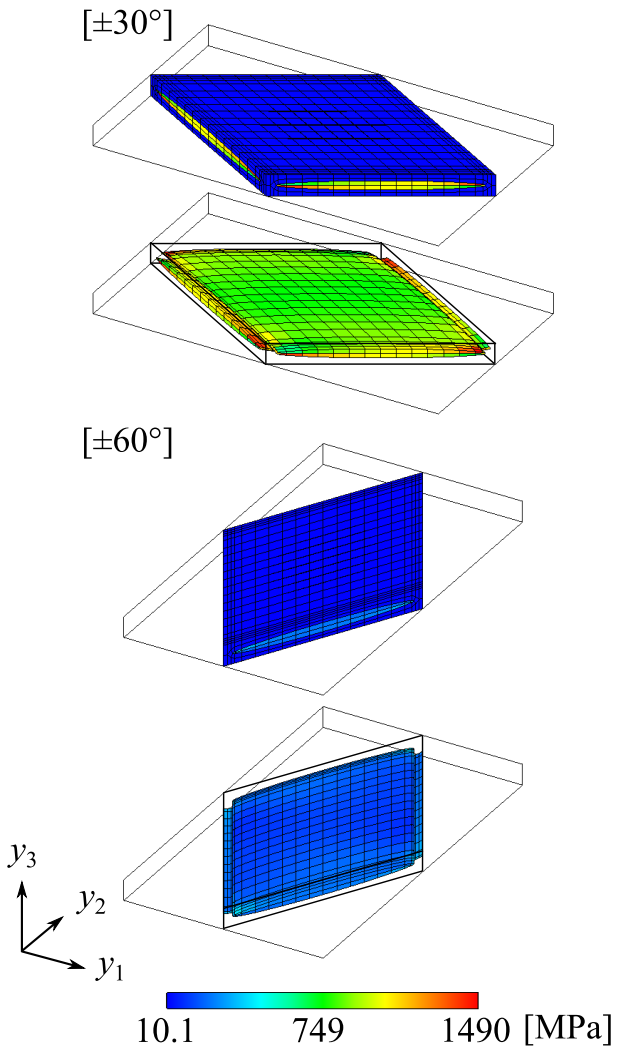

Figure 9: Distribution of microscopic Mises equivalent stress σ_{EQ} for [±30°] and [±60°] CF woven laminates at $E_{11} = 0.015$.

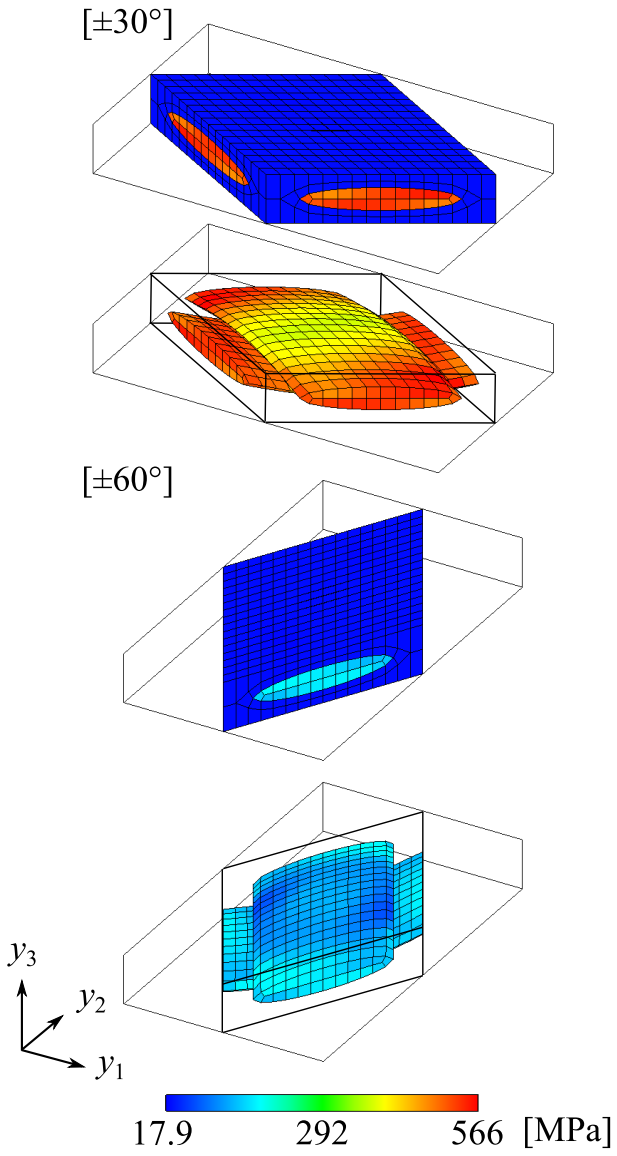

Figure 10: Distribution of microscopic Mises equivalent stress σ_{EQ} for [±30°] and [±60°] GF woven laminates at $E_{11} = 0.015$.

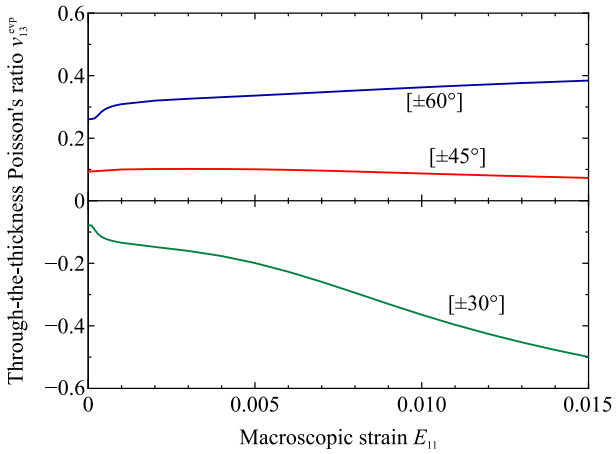

Figure 11: Relation between macroscopic strain and through-the-thickness Poisson's ratio ν_{13}^{evp} for $[\pm\theta]$ CF woven laminates.

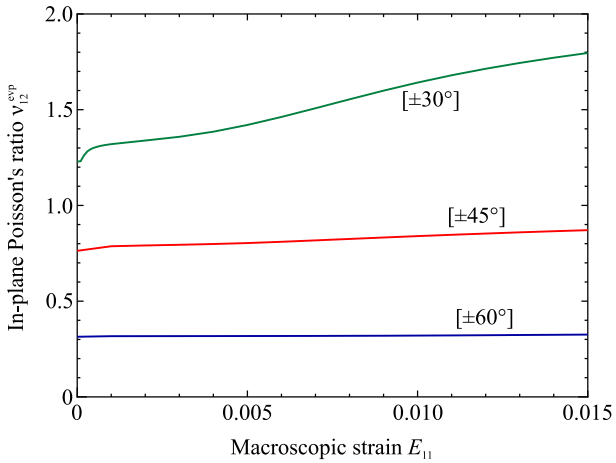

Figure 12: Relation between macroscopic strain E_{11} and in-plane Poisson's ratio ν_{12}^{evp} for $[\pm\theta]$ CF woven laminates.

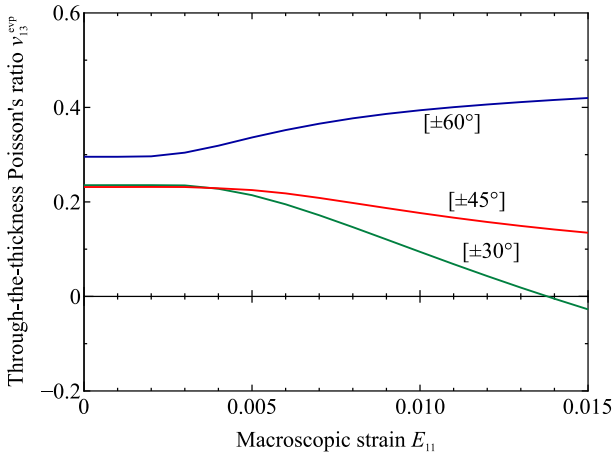

Figure 13: Relation between macroscopic strain and through-the-thickness Poisson's ratio ν_{13}^{evp} for $[\pm\theta]$ GF woven laminates.

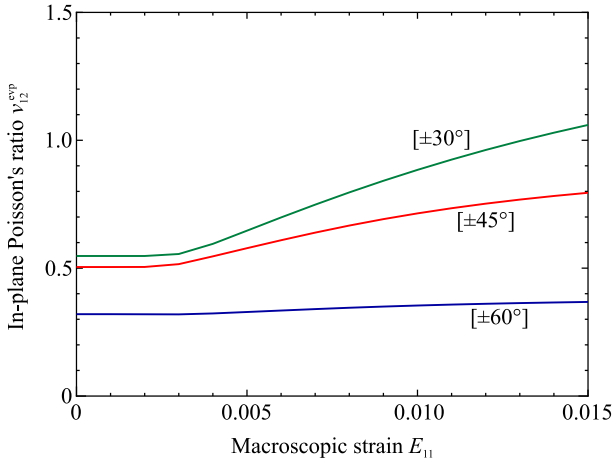

Figure 14: Relation between macroscopic strain E_{11} and in-plane Poisson's ratio ν_{12}^{evp} for $[\pm\theta]$ GF woven laminates.

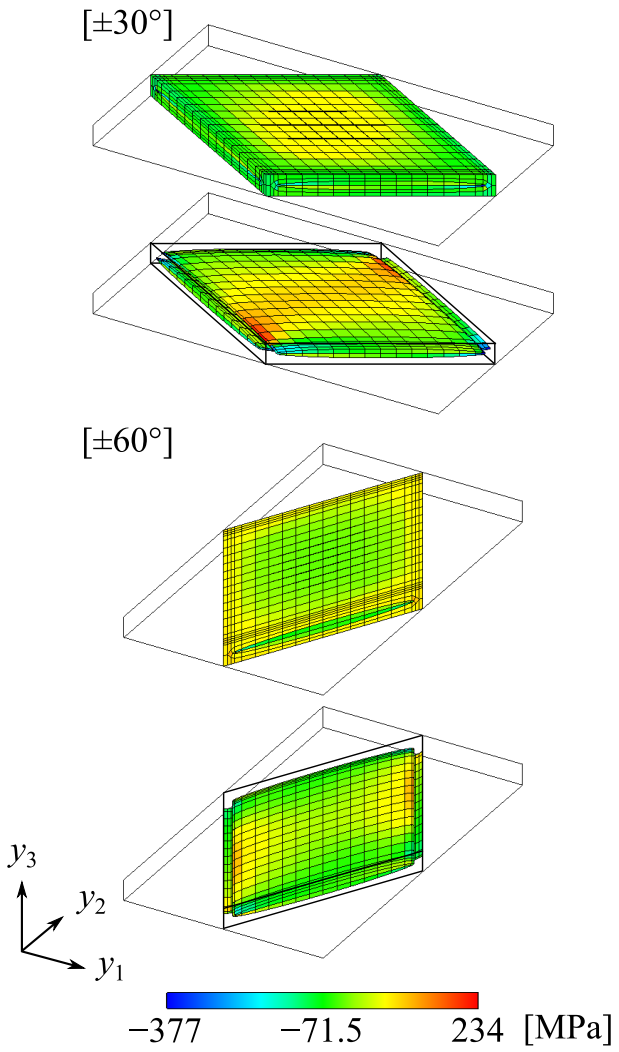

Figure 15: Distribution of microscopic stress σ_{22} for [±30°] and [±60°] CF woven laminates at $E_{11} = 0.015$.

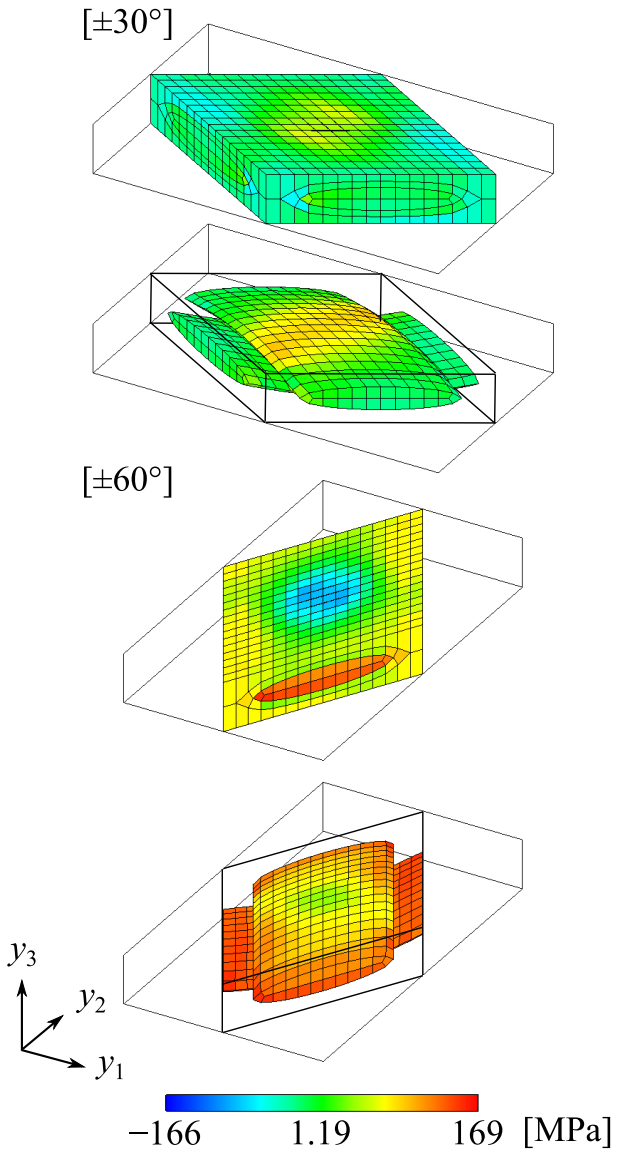

Figure 16: Distribution of microscopic stress σ_{22} for $[\pm 30^\circ]$ and $[\pm 60^\circ]$ GF woven laminates at $E_{11} = 0.015$.